RSC Advances

PAPER

View Article Online
View Journal | View Issue

Check for updates

Cite this: *RSC Adv.*, 2022, **12**, 11207

Facile fabrication of a phosphonium-based ionic liquid impregnated chitosan adsorbent for the recovery of hexavalent chromium†

Mochamad Lutfi Firmansyah, *[a] Thalabul Ilmi,[b] Rino Rakhmata Mukti,[bcd] Patmawati[e] and Masahiro Goto [fg]

Chitosan adsorbents impregnated with a phosphonium-based ionic liquid (Chi_IL), trioctyldodecyl phosphonium chloride, were prepared for the adsorption of hexavalent chromium and compared to the performance of native chitosan. The physical and chemical properties of the adsorbents were characterized by Fourier-transform infrared spectroscopy, X-ray diffraction, scanning electron microscopy, and energy-dispersive X-ray spectroscopy. Effects of various parameters, such as pH, adsorbent dosage, contact time, temperature, and multi-component systems, were systematically examined. Chi_IL showed a high adsorption capacity (282.6 mg g^{-1}) compared to native chitosan (238.1 mg g^{-1}). The adsorption kinetics of the metals followed a pseudo-second-order kinetic model, and the experimental data were a good fit for the Freundlich isotherm model. Following the isotherm and activation energy parameter, adsorption of Cr(VI) onto Chi_IL follows a chemisorption process, possibly through an anionic exchange with the anion of the IL. The thermodynamic parameters suggested that the adsorption of Cr(VI) is a spontaneous and exothermic reaction. In the column adsorption, Chi_IL exhibited a longer column exhaustion time than that of native chitosan owing to the enhanced adsorption capacity caused by the introduction of IL. Moreover, the column with the parameters of 6 cm bed depth, 5 mL min^{-1} flow rate, and 50 mg L^{-1} was able to achieve the best performance in Cr(VI) adsorption.

Received 5th January 2022
Accepted 4th April 2022

DOI: 10.1039/d2ra00064d

rsc.li/rsc-advances

Open Access Article. Published on 11 April 2022. Downloaded on 9/19/2024 3:12:51 PM.
This article is licensed under a Creative Commons Attribution-NonCommercial 3.0 Unported Licence.

Introduction

Heavy metals in wastewater have been an environmental concern for many years because of their harmful effect on human health and impact on other organisms; they are also considered non-biodegradable.[1] Industrial discharge, such as that from smelting, cosmetics, and stabilizers, and also effluence from domestic households introduce these metals into the environment through wastewater.[2] The main heavy metal pollutants in wastewater are known to be arsenic (As), cobalt (Co), chromium (Cr), cadmium (Cd), and lead (Pb), with Cr(VI) being widely used in many industrial applications. According to Indonesia's regulations, the permissible limits of Cr(VI) in industrial and domestic wastewater are 0.4 and 1 mg L^{-1}, respectively.[3] Cr(VI) accumulates in soils and living organisms and can cause various health issues, ranging from simple skin irritation to lung carcinoma.[4] In addition, Cr(VI) is known to be highly mobile in soils and in aquatic systems.

Adsorption methods have been widely used as an effective method for removing and separating metals.[5] Operation costs and user friendliness are some of the advantages of the adsorption process, and the current trend is toward cheap and abundant nonconventional bio-sorbents with a high removal efficiency.[6] However, the lack of adequate regeneration methods and the difficulty of handling spent adsorbents are among the limitations of adsorption processes. In recent years, there has been increased interest in the use of biopolymers, such as cellulose and chitosan, as alternative adsorbents because of their low cost and abundance and advantageous properties, such as their antibacterial activity, nontoxicity, biocompatibility, biodegradability, hydrophilicity, and high adsorption capacity.[7] Chitosan has been used in a number of metal

[a]*Nanotechnology Engineering, Faculty of Advanced Technology and Multidiscipline, Airlangga University, Jl. Dr Ir. H. Soekarno, Surabaya 60115, Indonesia. E-mail: ml.firmansyah@ftmm.unair.ac.id*

[b]*Division of Inorganic and Physical Chemistry, Faculty of Mathematics and Natural Science, Institut Teknologi Bandung, Jl Ganesha 10, Bandung 40132, Indonesia*

[c]*Research Center for Nanoscience and Nanotechnology, Institut Teknologi Bandung, Jl Ganesha 10, Bandung 40132, Indonesia*

[d]*Research and Innovation Center for Advanced Materials, Institut Teknologi Sumatera, Jl. Terusan Ryacudu, Lampung 35365, Indonesia*

[e]*Department of Marine, Faculty of Fisheries and Marine, Universitas Airlangga, Jalan Mulyorejo Kampus C, Surabaya 60115, Indonesia*

[f]*Department of Applied Chemistry, Graduate School of Engineering, Kyushu University, 744 Motooka, Nishi-ku, Fukuoka 819-0395, Japan*

[g]*Center for Future Chemistry, Kyushu University, 744 Motooka, Nishi-ku, Fukuoka 819-0395, Japan*

† Electronic supplementary information (ESI) available. See https://doi.org/10.1039/d2ra00064d

© 2022 The Author(s). Published by the Royal Society of Chemistry

Open Access Article. Published on 11 April 2022. Downloaded on 9/19/2024 3:12:51 PM.
This article is licensed under a Creative Commons Attribution-NonCommercial 3.0 Unported Licence.

adsorption studies.[8] Its chemical structure is modifiable, and a large number of applications are improved by modifying its properties. Modification of the chitosan molecule has been explored through grafting or crosslinking, which enhance its properties. Chitosan has been successfully impregnated with hydrogel, surfactant, and ionic liquid (IL) for various applications, such as catalysis, support materials, and adsorption.[8–10] Furthermore, the impregnation of chitosan with IL can alleviate most of the IL's disadvantages. IL has various attractive properties, such as being nonvolatile, thermally stable, and miscible in organic and aqueous solutions; however, it has a low mass transfer rate and may be lost into the aqueous system during adsorption operations.

In recent years, there has been increasing interest in IL-impregnated chitosan (chitosan-IL) because of its adsorption applications. Kumar *et al.* reported the immobilization of tetraoctylammonium bromide on chitosan for Cr(VI) adsorption.[11] This adsorbent demonstrates excellent performance due to the cooperative effect of both IL and chitosan, and it was easily regenerated with ammonium hydroxide. Moreover, Shekawat *et al.* reported the enhanced adsorption capacity of chitosan-IL by crosslinking it with sulfate.[12] Chitosan-IL has also been applied to the adsorption of Cr(VI), Hg(II), Ce(II), Sr(II), and Mo(II).[13,14] Aside from metal adsorption, chitosan-IL has also been used in the removal of dyes and herbicides.[15,16] Lin *et al.* reported an interesting application for the immobilization of IL using a chitosan-based capsule.[17] IL capsules require nontoxic and harmless natural macromolecule materials (chitosan, sodium alginate, *etc.*), which reduce their environmental impact. The volume of these capsules is generally large, which makes separation easier; however, it seems that the issue of adsorption regeneration has not yet been resolved for this capsule.

A number of studies have explored ammonium- and imidazolium-based IL in relation to the chitosan-IL adsorbent because of their inherent ability to interact with the chitosan structure. However, phosphonium-based IL has not been explored in this context. Phosphonium-based IL is typically stable compared with ammonium- or imidazolium-based IL, and it is also more stable under acidic and basic conditions owing to the absence of acidic protons.[18] Lin *et al.* reported the use of trihexyldodecylphosphonium chloride in the chitosan-capsule adsorbent.[17] In the present study, chitosan adsorbent impregnated with a phosphonium-based IL (Chi_IL), trioctyldodecyl phosphonium chloride, was synthesized and used as the separation tool for Cr(VI) in batch and column adsorption process. The effects of different parameters on adsorption performance, including adsorbent dosage, pH, and temperature, were investigated. In addition, adsorption kinetics, isotherms, and thermodynamics were studied comprehensively.

Experimental

Materials

Trioctylphosphine (97%) and 1-chlorododecane (97%), used as precursors for trioctyldodecyl phosphonium chloride ($P_{8,8,8,12}Cl$), were obtained from Sigma Aldrich (Tokyo, Japan) and Tokyo Chemical Industry Co., Ltd (Tokyo, Japan), respectively. HCl (5 mol L^{-1}), 1,5-diphenylcarbazide (DPC, 98%), and chromium(VI) standard solutions (1000 mg L^{-1}) were purchased from Merck. Locally source chitosan (Crab from Cirebon, Indonesia) was provided by Chimultiguna (Indonesia, deacetylation degree of 86.94%), and acetone was purchased from Himedia (India).

Preparation of $P_{8,8,8,12}Cl$-impregnated chitosan (Chi_IL)

An IL, trioctyldodecyl phosphonium chloride ($P_{8,8,8,12}Cl$), was prepared as reported previously.[19] The preparation of chitosan impregnated with ILs was performed as planned in the previous report.[20] Initially, chitosan was crosslinked with sulfate by mixing 5 g of chitosan and 100 mL of 1 mol L^{-1} H_2SO_4 and then stirring the mixture for 1 h. The residue was washed and air-dried at 333 K in an oven. The impregnation of chitosan by IL was conducted by mixing crosslinked chitosan (2.5 g) with 30 mL of $P_{8,8,8,12}Cl$ in acetone (0.05 mol). The mixture was then refluxed for 1 h at 323 K. The residue was washed and air-dried at 333 K in an oven and used for further adsorption studies.

The chitosan impregnated with IL (Chi_IL) was characterized using Fourier-transform infrared spectroscopy (FTIR), X-ray diffraction (XRD), scanning electron microscopy (SEM), and energy-dispersive X-ray spectroscopy (EDX). The FT-IR measurement was recorded using the Shimadzu FT-IR Affinity-1 spectrometer in the range of 500–4000 cm^{-1} with a resolution of 1 cm^{-1}. The crystalline structure of the catalysts was studied using XRD and recorded on a Bruker D2 Phaser X-ray diffractometer using Cu Kα radiation with an increment of 1° per second. The Chi_IL morphology and elemental composition were characterized through an SEM/EDX analysis on the Phenom Desktop ProXL.

Metal concentration measurements

The determination of metal concentrations was carried out using the spectrophotometric method. Diphenylcarbazide (DPC) was used as a complexing agent for Cr(VI); the DPC–Cr(VI) complex becomes bright purple when the absorbance peak reaches 540 nm.[21] All the experiments and spectrophotometric measurements were conducted in triplicate to minimize errors, which did not exceed 4%. Spectrophotometric analysis was performed with a Hinotek N4S UV-Vis Spectrophotometer (Ningbo Hinotek Technology Co., Ltd, China). The absorbance of the solutions was measured using a 1 cm-thick quartz cell against double-distilled water as a blank, unless stated otherwise. The metal-containing solution with concentrations in the range of 50–150 mg L^{-1} was mixed with the appropriate color-developing reagents. The absorbance of the Cr(VI)-containing solution was then measured at 540 nm.

Adsorption procedure

Batch adsorption. The adsorption experiment was carried out by mixing 0.2 g of adsorbent with a 50 mL metal-containing solution (100 mg L^{-1}) at 298 K for a 90 min. The metal concentration in the solution was determined using a UV

© 2022 The Author(s). Published by the Royal Society of Chemistry

Open Access Article. Published on 11 April 2022. Downloaded on 9/19/2024 3:12:51 PM.
This article is licensed under a Creative Commons Attribution-NonCommercial 3.0 Unported Licence.

spectrophotometer. The adsorption efficiency and equilibrium adsorption capacity (q_{eq}) were calculated as follows:

$$E\,(\%) = ((C_i - C_{eq})/C_i) \times 100 \quad (1)$$

$$q_{eq} = ((C_i - C_{eq})/W) \times V \quad (2)$$

where C_i and C_{eq} refer to the metal concentration (mg L^{-1}) in the initial and equilibrium states, respectively, and V and W are the volume of the metal-containing solution and the weight of the adsorbent, respectively. All experiments were conducted in triplicate to obtain reliable data.

Column adsorption. Column adsorption experiment was performed in a glass column with a length 30 and 2.0 cm internal diameter at the temperature of 298 K. The column was packed according to Fig. 1. Glass wool which could aid as a filter aid provided at the top and bottom of the column. The adsorbent was placed from top to bottom and then covered glass beads (5 mm) to ensure the influent was distributed properly. Peristaltic pump was used to pump the influent solution at a controlled flow rate. Parameters, such as bed depth (4, 5, and 5 cm), flow rate (5, 10, 15 mL min^{-1}) and influent concentration (50, 100, 200 mg L^{-1}) were investigated. The effluent was sampled at regular intervals of ten minutes.

The value of effluent volume (V_{eff}, mL), total mass of metal adsorbed (q_{tot}, mg), maximum uptake (q_{eq}, mg g^{-1}), total amount of metal entering column (m_{tot}, mg) and Cr(VI) removal efficiency (E, %) can be calculated from the eqn (3)–(7), respectively.

$$V_{eff} = Qt_{tot} \quad (3)$$

$$q_{tot} = (Q/1000)\int_{t=0}^{t=tot} C_{ad}\,dt \quad (4)$$

$$q_{eq} = (q_{tot}/m) \quad (5)$$

$$m_{tot} = (C_i Q t_{tot})/1000 \quad (6)$$

$$E\,(\%) = (q_{tot}/m_{tot}) \times 100 \quad (7)$$

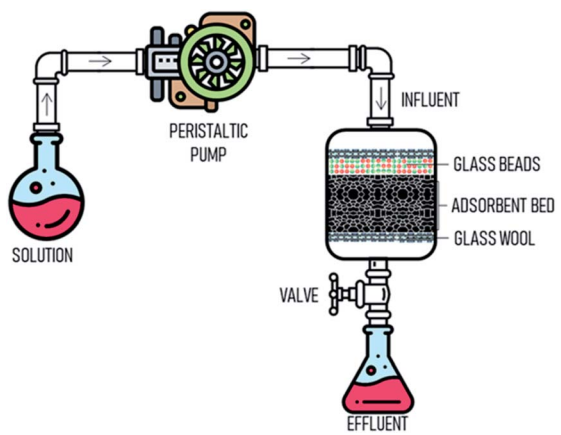

Fig. 1 The schematic drawing of the fixed-bed adsorption column for experimental study.

where Q is the volumetric flow rate (mL min^{-1}), t_{tot} is the total flow time (min) and C_{ad} is the concentration of metal removal (mg L^{-1}).

Results and discussions

Physicochemical characterization of the adsorbent

The structural and morphological analysis of chitosan and Chi_IL were carried out using an XRD and SEM analyses, respectively. As shown in Fig. 2A, the amorphous nature of chitosan was reflected in the XRD patterns, and chitosan characteristic peaks were also observed at $2\theta = 12.12°$, 19.55°, and 23.45° in both chitosan and Chi_IL diffraction.[22] In the Chi_IL diffraction pattern, the characteristic peaks of chitosan shifted slightly to 19.37°. Chi_IL also showed a lower intensity in the chitosan characteristic peaks than that of chitosan, which indicates a decrease in crystallinity due to the interaction between $P_{8,8,8,12}Cl$ and chitosan.

The chemical interactions and footprints of the adsorbents were examined with a FTIR spectrophotometer (Fig. 2B). In the chitosan spectra, the presence of maxima at 3400 cm^{-1} was assigned to O–H and N–H stretching vibrations. Moreover, N–H bending and C–H, C–O, and C=O stretching vibrations were observed at 1569, 2880, 1154, and 1657 cm^{-1}, respectively.[14,23] Changes were observed after the impregnation process, such as the shifting and broadening of the hydroxyl peak from 3400 to 3451 cm^{-1}. Moreover, shifting also occurred in the C–N bending vibrations from 1375 to 1359 cm^{-1}, and the occurrence of two additional peaks at 2938 and 2881 cm^{-1} was assigned to the IL C–H_2.[24] New peaks were observed in the Chi_IL FT-IR spectra, which could be ascribed to the P–C vibrations originating in the cationic moieties of $P_{8,8,8,12}Cl$. Peaks at 1421 and 732 cm^{-1} were ascribed to P–C deformation and stretching vibrations, respectively.[24] Upon the adsorption of metal ions, shifts in the P–C characteristic peak were observed from 1421 to 1398 cm^{-1} and 732 to 710 cm^{-1} (Fig. S2†). This result could be interpreted as the adsorption of metal ions through their coordination with $P_{8,8,8,12}Cl$ cationic moieties due to an electrical interaction.

Fig. 3 shown the morphology of chitosan and Chi_IL post adsorption. Chitosan morphology exhibits a dense and uneven surface, and there are no observable visual changes in the chitosan morphology upon IL impregnation or metal adsorption.

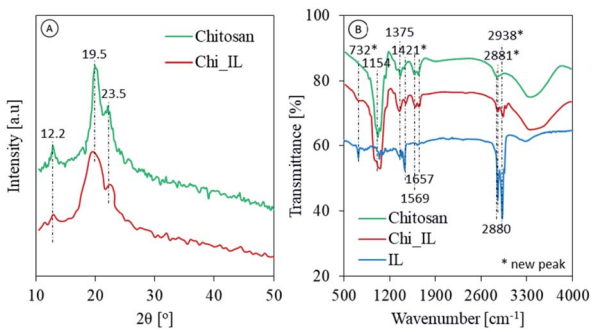

Fig. 2 (A) Diffraction pattern and (B) FTIR spectrum of chitosan and Chi_IL.

Open Access Article. Published on 11 April 2022. Downloaded on 9/19/2024 3:12:51 PM.
This article is licensed under a Creative Commons Attribution-NonCommercial 3.0 Unported Licence.

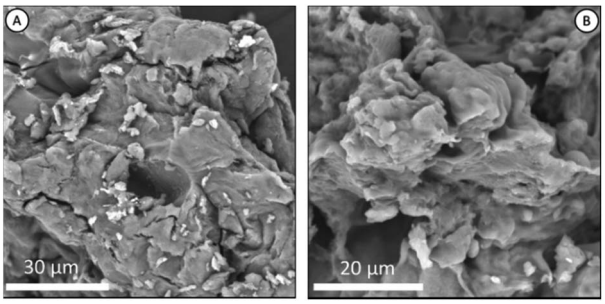

Fig. 3 (A) SEM image of native chitosan, and (B) SEM image of Chi_IL post-adsorption.

Post-impregnation and post-adsorption Chi_IL showed the presence of phosphorus atoms that originate from the cationic center of $P_{8,8,8,12}Cl$ and Cr(VI) (Fig. S1†).

Adsorption behavior

Speciation of adsorbate and surface charge of adsorbent depends upon pH of the solution. Hence, it is customary to study pH effect on adsorption efficiency. In the present study, 50 mL of 100 mg L^{-1} of Cr(VI) solutions were equilibrated with 300 mg of Chi_IL. The pH of the solutions was varied from 2.0 to 10.0. As shown in Fig. 4A, the highest adsorption efficiency of Cr(VI) was achieved at pH of 4.0. Cr(VI) complexes in aqueous solution mainly exists in the form of $HCrO_4^-$, $Cr_2O_7^{2-}$, and CrO_4^{2-}. The equilibrium between these complexes was presented as follows:

$$H_2CrO_4 \leftrightharpoons H^+ + HCrO_4^- \quad (8)$$

$$2HCrO_4^- \leftrightharpoons Cr_2O_7^{2-} + H_2O \quad (9)$$

$$HCrO_4^- \leftrightharpoons H^+ + CrO_4^{2-} \quad (10)$$

Following the UV-vis spectra, Cr(VI) containing solution in acidic condition shows two peak at 255 and 345 nm. While, the solution in basic and neutral condition shows two peak at 270 and 370 nm, indicating the presence of difference Cr(VI) complexes in both condition (Fig. S3A†).[25,26] CrO_4^{2-} mainly exists in basic and neutral condition. While, $HCrO_4$- and $Cr_2O_7^{2-}$ mainly exists in acidic condition.[27] The solution in different pH also showed a different color (Fig. S3B†). The acidic Cr(VI) solution showed a yellow color, while basic Cr(VI) solution showed an amber color. The adsorption of Cr(VI) by Chi_IL could be done through electrostatic interaction between the anionic complex and the amine through the exchange with the sulfate group or with the IL through the anionic exchange.[28] A notable decrease was observed after the pH was increased to 6. This could be due to the change in the surface charge of the adsorbent since the pH_{pzc} of Chi_IL was found to be 4. The pH_{pzc} was determined by using pH drift method as reported by Jiao *et al.*[29] The pH_{pzc} reflect the surface charge of the materials at certain pH. Material will have positively charged surface in pH below the pH_{pzc} and negatively charged above it.

Assessing the effective adsorbent dose is paramount when measuring adsorbent potential within a certain concentration range. Thus, chitosan and Chi_IL doses were varied from 50 to 500 mg to investigate the effect of different doses on adsorption efficiency. As shown in Fig. 4C, the adsorption of Cr(VI) increased linearly with the increased adsorbent dose. Chi_IL was able to reach equilibrium at lower dose than that of chitosan, which is 300 mg. Chitosan achieved above 95% adsorption efficiency also at 300 mg. Beyond 300 mg, there was a little to no observable changes in the removal of Cr(VI) owing to the saturation of the active adsorption sites. Therefore, 300 mg of adsorbent dose was used for the rest of the adsorption studies.

The desorption of Cr(VI) from both adsorbent was done by using 0.005 mol L^{-1} HCl. The desorption efficiency of both chitosan and Chi_IL reached 90%. After the desorption, the adsorbent was thoroughly washed with deionized water and regenerated with 0.01 mol L^{-1} NaCl solution. The regenerated adsorbent was used in the further adsorption–desorption cycle investigate its regenerability. The test was done in 3 cycle. Considering the accumulated Cr(VI) in the adsorbent, the Chi_IL showed a 10% decrease in the efficiency after three cycles (Fig. S4†). While, chitosan showed a notable decrease in the 2nd cycle.

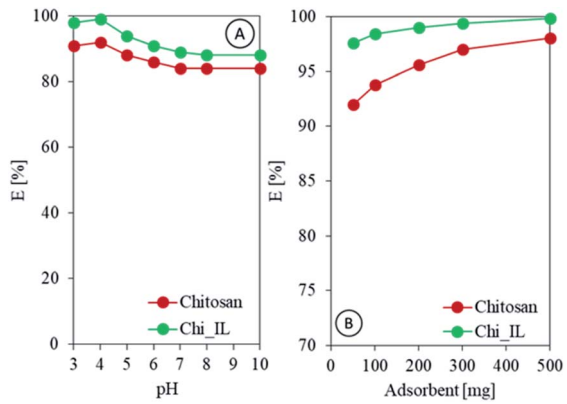

Fig. 4 (A) Effect of pH on the adsorption efficiency of Cr(VI), and (B) effect of the adsorbent dose on the adsorption efficiency of Cr(VI).

Adsorption kinetics

The contact time of the experiment was varied from 10 to 90 min to analyze the adsorption kinetics of Cr(VI). Chi_IL was able to reached equilibrium in Cr(VI) adsorption in 60 minutes, while chitosan achieved the equilibrium in 90 minutes. Thus, 90 minutes was then used in further experiments. Moreover, pseudo-first-order and pseudo-second-order kinetic models were applied to determine the number of metal ions adsorbed at various contact times and their kinetic parameters, as shown in eqn (11) and (12):[30,31]

$$q_t = q_e(1 - e^{-K_1 t}) \quad (11)$$

$$q_t = K_2 q_{eq}^2 t/(1 + K_2 q_{eq} t) \quad (12)$$

© 2022 The Author(s). Published by the Royal Society of Chemistry

Open Access Article. Published on 11 April 2022. Downloaded on 9/19/2024 3:12:51 PM.
This article is licensed under a Creative Commons Attribution-NonCommercial 3.0 Unported Licence.

Both equations were transformed to their linear form according to the following equations:

$$\log(q_{eq} - q_t) = \log q_{eq} - (K_1 t/2.303) \quad (13)$$

$$(t/q_t) = 1/K_2 q_{eq}^2 + t/q_{eq} \quad (14)$$

where q_{eq} and q_t are the amount of Cr(VI) adsorbed at the equilibrium and at the specified time t, respectively, and K_1 and K_2 are the rate constant of the pseudo-first-order and pseudo-second-order rate, respectively. The linear correlation between $\log(q_{eq} - q_t)$ and t provides the pseudo-first-order rate constant, and the linear correlation between t/q_t and t provides the pseudo-second-order rate constant.

Table 1 shows the adsorption kinetic parameters of Cr(VI) by chitosan and Chi_IL. The pseudo-second-order parameters fit well with the adsorption kinetics of Cr(VI) by both adsorbents, as they showed the closest calculated q_e values to Cr(VI) and the highest correlation coefficient (R^2). The faster adsorption of Cr(VI) by Chi_IL was also reflected in the kinetic constant, which shows that the kinetic constant of Chi_IL was higher than that of chitosan. The higher kinetic of Chi_IL could be contributed by the presence of IL that could enhanced adsorption through electrostatic interaction with the metal ions.[12] Moreover, the activation energy (E_a) can be obtained with the linearized Arrhenius equation, which is shown in eqn (15).

$$\ln K_t = \ln A - (E_a/RT). \quad (15)$$

With the suitability of pseudo-second order kinetic model, the calculation of E_a was done by using the coefficient of K_2. The E_a of Cr(VI) adsorption for chitosan and Chi_IL that was calculated from the linear plot between ln *K vs. 1/T* (Fig. S5†), were 71.7 and 59.8 kJ mol^{-1}, respectively. Since the E_a values was higher than that of 40 kJ mol^{-1}, the Cr(VI) ions was chemically adsorbent onto the adsorbents.[32] The E_a of Chi_IL was lower than that of chitosan due to the presence of $P_{8,8,8,12}Cl$ which provide additional adsorption sites for the Cr(VI). The E_a also a crucial aspect in the determination of the reaction rate. The reaction was consider as quick with E_a less than 40 kJ mol^{-1} and slow with E_a more than 120 kJ mol^{-1}.[33] Thus, the adsorption of Cr(VI) by both adsorbent was not particularly fast reaction due to the chemical adsorption process.

Table 1 Kinetic parameters for the adsorption of Cr(VI) onto adsorbents

		Adsorbent	
Kinetic model	Parameters	Chitosan	Chi_IL
Pseudo-first order	K_1	0.041	0.054
	$q_{e,exp}$	12.31	12.45
	$q_{e,cal}$	8.99	7.68
	R^2	0.9480	0.9967
Pseudo-second order	K_2	0.072	0.092
	$q_{e,exp}$	12.31	12.45
	$q_{e,cal}$	12.26	12.43
	R^2	0.9995	0.9999
Intraparticle diffusion	K_{int}	0.174	0.278
	R^2	0.8858	0.8872

In addition, the diffusion model involved in the adsorption of Cr(VI) was explored with the intraparticle diffusion model. The Weber–Morris equation was used to explain this model:[34]

$$q_t = -K_{int} t^{1/2} + C \quad (16)$$

where q_t (mg g^{-1}) and K_{int} (mg g^{-1} min$^{-1/2}$) represent the amount of metal adsorbed at a certain time and the intraparticle diffusion rate constant, respectively. The value k_{int} was obtained from the slope of q_t *versus* the $t_{1/2}$ plot. The calculated K_{int} for Cr(VI) was presented in Table 1. Cr(VI) show a nonzero intercept, demonstrating that there are further factors contributing to the rate-limiting step aside from the diffusion process.

Adsorption isotherms

Chitosan and Chi_IL were subjected to adsorption of Cr(VI) at a different initial concentration in the range of 50–700 mg L^{-1} with 50 mg L^{-1} interval. Chi_IL showed a slight decrease in the adsorption efficiency, which was 98.8 to 96.7%, after the concentration of 200 mg L^{-1}, while chitosan showed a higher decrease in adsorption efficiency, which was 96.8 to 91.1%, after the concentration of 100 mgL^{-1}. The lesser decrease in Chi_IL than that of chitosan could be attributed to the presence of IL which provided additional adsorption sites. The experimental data were then fitted to several adsorption isotherm models, such as the Langmuir, Freundlich, Temkin, and Frenkel–Helsey–Hill (FHH) models, and the correlation coefficient (R^2) was used to determine the most suitable isotherm model for adsorption.

Typically, monolayer adsorption is explained by the Langmuir isotherm model.[35,36] A linearized Langmuir equation (eqn (17)) presents the maximum adsorption capacity (q_0, mg g^{-1}) and the Langmuir constant (b, L mg^{-1}), which was obtainable from the plot of C_{eq}/q_{eq} *versus* C_{eq}:

$$(C_{eq}/q_{eq}) = (1/q_0 b) + (C_{eq}/q_0) \quad (17)$$

Moreover, the Langmuir constant is related to the separation factor (R_L), which reflects the effectiveness of adsorption and is given by the following equation:

$$R_L = 1/(1 + bC_0) \quad (18)$$

where R_L indicates the favorability of the adsorption process ($R_L = 0$: irreversible adsorption, $0 < R_L > 1$: favorable adsorption, $R_L = 1$: linear adsorption, and $R_L > 1$: unfavorable adsorption).[37]

Multilayer adsorption was modeled with the Freundlich and FHH isotherm models.[38] The linearized equations for both models are presented in eqn (19) and (20):

$$\log q_{eq} = \log k_F + (1/n)\log C_{eq} \quad (19)$$

$$\ln q_{eq} = (1/n)\ln K + (1/n)\ln C_{eq} \quad (20)$$

The Freundlich adsorption parameters, such as adsorption capacity (K_F, mg$^{1-1/n}$ g^{-1} L^{-1}) and adsorption heterogeneity (n),

Open Access Article. Published on 11 April 2022. Downloaded on 9/19/2024 3:12:51 PM.
This article is licensed under a Creative Commons Attribution-NonCommercial 3.0 Unported Licence.

were obtained from the plot of log q_{eq} against log C_{eq} (eqn (10)). The FHH adsorption parameters, such as the FHH constant (K) and adsorption intensity ($1/n$), were obtained from the plot of ln q_{eq} against ln C_{eq} (eqn (11)). In both isotherm models, the values n and $1/n$ indicate the interaction between the adsorbent and the adsorbate.[36,38]

The Temkin isotherm explores the adsorbent–adsorbate interaction, which decreases the adsorption heat in multilayer adsorption. Ignoring the low and high thresholds of the concentrations, the Temkin model assumes a linear decrease in the heat of adsorption with an increase in the layers of adsorbate.[31] The linearized Temkin equation is expressed as follows:

$$q_{eq} = \beta \ln A_T + \beta \ln C_{eq} \quad (21)$$

The Temkin adsorption parameters, such as the equilibrium binding constant (A_T, L g^{-1}) and heat of adsorption (β, kJ mol L^{-1}), were obtained from the slope and intercept of the plot of q_{eq} against ln C_{eq}. The Temkin constant (b_T), which clarifies the adsorption process (b_T > 40 kJ mol^{-1} = chemisorption process, b_T < 40 kJ mol^{-1} = physisorption process),[39] was obtained from the following equation

$$\beta = RT/b_T \quad (22)$$

According to the comparison of the regression coefficient, multilayer adsorption was a suitable fit for the sorption of Cr(VI) by both chitosan and Chi_IL. In agreement with the adsorption results, Chi_IL showed higher adsorption capacity than that of chitosan, which could be attributed to the native adsorption sites and the presence of $P_{8,8,8,12}Cl$.

Following the Langmuir model, chitosan and Chi_IL showed separation factor less than unity (Table 2), which indicates the effective interaction between the Cr(VI) ions and both chitosan and Chi_IL. According to both the Freundlich and FHH isotherm models, the n-factor values were between 1 and 10, which indicates beneficial adsorption for Cr(VI), and the small value of $1/n$ (0.50 for chitosan and 0.49 for Chi_IL) signifies an active interaction between both components. The Temkin constant (b_T) from the adsorption of Cr(VI) by chitosan and Chi_IL was higher than 40 kJ mol^{-1}, which means that the adsorption of Cr(VI) followed the chemisorption pathway. Fig. 5 shows the isotherm fit between the experimental data with Langmuir and Freundlich models. In agreement with the regression coefficient, the experimental data fitted better to the Freundlich isotherm models. Thus, the adsorption of Cr(VI) by both adsorbent followed a multilayer chemisorption pathway with a beneficial interaction between components.

Table 2 Isotherm parameters for the adsorption of Cr(VI) onto Chi_IL

Isotherms models	Parameters	Chi_IL	Chitosan
Langmuir	q_0	282.6	238.1
	B	0.076	0.050
	R^2	0.9641	0.9025
	R_L	0.2075–0.0183	0.2852–0.0277
Freundlich	K_F	34.92	16.75
	N	2.00	1.97
	R^2	0.9905	0.9900
Temkin	A_T	1.46	2.24
	b_T	45.23	52.33
	β	54.77	47.33
	R^2	0.9419	0.8686
Frenkel-Helsey Hill	K	0.0008	0.0038
	n	2.00	1.97
	R^2	0.9905	0.9800

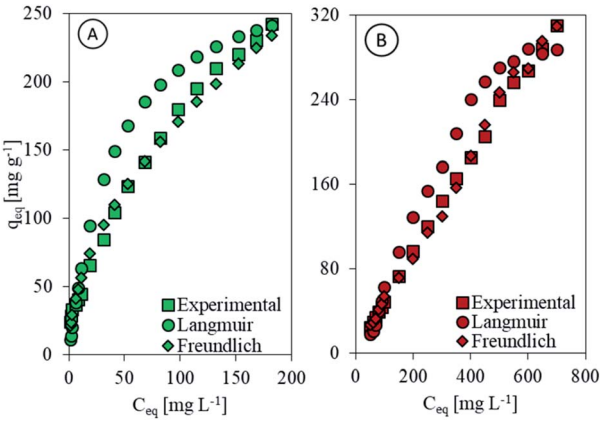

Fig. 5 Comparison of experimental data with Langmuir and Freundlich model for (A) chitosan and (B) Chi_IL.

Adsorption thermodynamics

Temperature is a critical parameter that has a perceivable influence over the adsorption performance of an adsorbent.[40] The adsorption of Cr(VI) was studied under the isothermal condition at a temperature range of 298–328 K and pH of 4. The thermodynamic parameters, such as the Arrhenius activation energy (E_a, kJ mol^{-1}), Gibbs free energy (ΔG, kJ mol^{-1}), enthalpy change (ΔH, kJ mol^{-1}), and entropy change (ΔS, J mol^{-1} K^{-1}), were determined from the experimental data. These parameters were calculated (given in Table 3) using following Van't Hoff equation:[41,42]

$$\Delta G = -RT \ln K_D. \quad (23)$$

A combination of eqn (21) and (22) gives a linearized form for the Van't Hoff plot (eqn (23)), which then provides ΔH and ΔS from the slope and the intercept of the plots[41,42]

$$\Delta G = \Delta H - T\Delta S, \quad (24)$$

$$\ln K_D = (\Delta S/R) - (\Delta H/RT), \quad (25)$$

where R (8.314 J mol^{-1} K^{-1}) and T (K) are the gas constant and temperature, respectively. The thermodynamic equilibrium constant (K_D) was obtained from the plots of ln(q_{eq}/C_{eq}) *versus* C_{eq} at various temperatures.[43,44] The adsorption of Cr(VI) demonstrated negative ΔH, negative ΔS, and negative ΔG, which indicates that the adsorption was exothermic and spontaneous with a high affinity for Cr(VI).[43]

© 2022 The Author(s). Published by the Royal Society of Chemistry

Open Access Article. Published on 11 April 2022. Downloaded on 9/19/2024 3:12:51 PM.
This article is licensed under a Creative Commons Attribution-NonCommercial 3.0 Unported Licence.

Table 3 Thermodynamic parameters of Cr(VI) adsorption onto adsorbents

T (K)		298	303	308	318	328
Chitosan	ΔG [kJ mol^{-1}]	−29.8	−29.8	−29.8	−29.7	−29.7
	ΔH [kJ mol^{-1}]	−32.4				
	ΔS [J mol^{-1} K^{-1}]	−8.4				
Chi_IL	ΔG [kJ mol^{-1}]	−57.1	−57.9	−56.7	−56.6	−56.5
	ΔH [kJ mol^{-1}]	−63.8				
	ΔS [J mol^{-1} K^{-1}]	−22.6				

Fixed-bed column adsorption

Table 4 shows the column adsorption parameters for the adsorption of Cr(VI) by chitosan and Chi_IL. The breakthrough time (t_b) and total flow time (t_{tot}) were defined as the time needed to achieve 5 and 95% of total influent concentration, respectively. Moreover, various parameters, such as the bed depth, the influent flow rate, and the initial Cr(VI) concentration were also assessed to determine the best parameter for the column adsorption. An increase in the bed depth provided a longer contact time between the adsorbate and the adsorbent which leads to a significant increase in t_b and t_{tot} (Table 4 and Fig. S6†). An increase in the bed depth also resulted in an increase in the amount of adsorbent. This leads to an increase in the total metal adsorbed (q_{tot}) and a decrease in the maximum uptake (q_{eq}) due to an increase in the adsorbent amount. On the other hand, the shorter residence time due to the increase in the flow rate negatively affected the t_{tot} and t_b, which cause almost 50% decrease in both value.[45] An increase in the flow rate also enhanced the total amount of metals in the column (m_{tot}), and q_{eq}. However, the highest adsorption efficiency was achieved at flow rate of 5 mL min^{-1} due to the column ability to retain equilibrium and sufficient contact time. Increase in the Cr(VI) initial concentration also negatively affected the t_b and t_{tot} due to higher concentration gradient driven up the adsorption kinetic. Moreover, the increase in the influent concentration also enhanced the m_{tot}, q_{tot}, and q_{eq} but not to a greater extent. However, Chi_IL showed significantly higher column capacity and uptake than that of chitosan regardless of the experimental conditions. This could be associated with the enhanced adsorption capacity of chitosan by the introduction of $P_{8,8,8,12}Cl$. The high hydrophobicity of $P_{8,8,8,12}Cl$ which could prevent the leakage of the IL into the aqueous phase, could also influenced the column exhaustion time.

Table 4 Column adsorption parameter for chitosan and Chi_IL

			Chitosan					Chi_IL				
C_i[a]	Q[b]	Z[c]	t_{tot}	m_{tot}	q_{tot}	q_{eq}	E	t_{tot}	m_{tot}	q_{tot}	q_{eq}	E
50	5	4	980	245	171	114	70	1320	330	309	206	94
50	5	5	1050	263	201	67	76	1470	368	341	114	93
50	5	6	1120	280	225	45	80	1560	390	371	74	95
50	5	6	1120	280	225	45	80	1560	390	371	74	95
50	10	6	840	420	254	51	60	1230	615	518	104	84
50	15	6	660	495	268	54	54	930	698	547	109	78
50	5	6	1120	280	225	45	80	1560	390	371	74	95
100	5	6	910	455	229	46	50	990	495	377	75	76
200	5	6	580	580	233	47	40	620	620	428	86	69

[a] mg L^{-1}. [b] mL min^{-1}. [c] cm.

In this study, Adams–Bohart, Thomas, and Yoon–Nelson models were developed to identify the best model for predicting the dynamic behavior of the column.[46] The equation for these models were presented in eqn (26)–(28).

$$\ln\left(\frac{C_t}{C_i}\right) = k_{AB}C_i t - k_{AB}N_0\left(\frac{Z}{U_0}\right) \quad (26)$$

$$\ln\left(\frac{C_i}{C_t} - 1\right) = \frac{k_{TH}q_{eq}m}{m} - k_{TH}C_i t \quad (27)$$

$$\ln\left(\frac{C_t}{C_i - C_t}\right) = k_{YN}t - \tau k_{YN} \quad (28)$$

where k_{AB} (L mg^{-1} min^{-1}) is the Adam–Bohart kinetic constant, N_0 (mg L^{-1}) is the saturation concentration, U_0 (cm min^{-1}) is the superficial velocity, k_{TH} (L mg^{-1} min^{-1}) is the Thomas kinetic constant, q_{eq} (mg g^{-1}) is the adsorption capacity, k_{YN} (L mg^{-1} min^{-1}) is the Yoon–Nelson kinetic constant, and τ (min) is the time for 50% breakthrough.

The breakthrough curve of both chitosan and Chi_IL showed a close fit with Thomas and Yoon–Nelson model (Fig. S6†). The R^2 values of the Thomas model (0.995–0.998) and Yoon–Nelson model (0.997–0.996) were larger than those of the Adam–Bohart model (0.789–0.822). In addition, both models also showed a close fit between calculated q_{eq} and τ value and experimental value (Table S1†). The τ value showed a good correlation between the availability of adsorbent and concentration gradient, which could indicated the influence of mass transfer over the adsorption process. The highest Cr(VI) adsorption efficiency by chitosan and Chi_IL was achieved at flow rate of 5 mL min^{-1}, bed depth of 6 cm and 50 mg L^{-1} of Cr(VI) solution. Following the results, it can be concluded that both Thomas and Yoon–Nelson model can predict the dynamic behavior of Cr(VI) adsorption by Chi_IL and chitosan.

Comparison with other chitosan-based adsorbents

The performance of chitosan and Chi_IL compared with previously reported materials was shown in Table 5. While,

Table 5 Comparison of Chi_IL with other reported materials

Adsorbent	Analyte	Adsorption capacity [mg g^{-1}]	Ref.
Chitosan	Cr(VI)	225.9	47
Chitosan	Cr(VI)	238.1	20
A336/chitosan	Pd(II)	187.6	48
Cyphos101/chitosan beads	Cr(VI)	104.4	17
Glutamic-IL/chitosan	Pb(II)	185.0	49
EPmim/chitosan	Re(VII)	149.2	50
Chitosan	Cr(VI)	238.1	This study
Chi_IL	Cr(VI)	282.6	

Open Access Article. Published on 11 April 2022. Downloaded on 9/19/2024 3:12:51 PM.
This article is licensed under a Creative Commons Attribution-NonCommercial 3.0 Unported Licence.

chitosan showed a similar capacity to other reports. Chi_IL has shown to possess a better adsorption capacity compared with other materials.

Conclusions

Chitosan and Chi_IL were prepared as adsorbent for Cr(VI). Chi_IL has shown an superior adsorption capacity for Cr(VI) with fast sorption kinetics than that of native chitosan. The adsorbent dosage, pH, initial concentration, contact time, and temperature were influential factors in the adsorption of Cr(VI). The adsorption of Cr(VI) onto the chitosan and Chi_IL probably proceeds by electrostatic static interaction with chitosan and anionic exchange with the $P_{8,8,8,12}Cl$. The adsorption process is thermodynamically favorable for the removal of Cr(VI) from synthetic effluents. Moreover, an exothermic multilayer chemisorption process was a good fit for the adsorption of Cr(VI) by both adsorbent. The pseudo-second-order kinetic model was also a good fit to this mechanism. Chi_IL showed a high adsorption capacity (282.6 mg g^{-1}), which could be contributed due to the presence of $P_{8,8,8,12}Cl$ in the Chi_IL. While, native chitosan showed an adsorption capacity of 238.1 mg g^{-1}. Moreover, chitosan and Chi_IL also performed well in column adsorption experiment. Chi_IL was able to achieve longer column exhaustion time than that of native chitosan due to the enhanced adsorption capacity as well as high hydrophobicity of $P_{8,8,8,12}Cl$ that prevent leakage of IL onto the mobile phase. The best performance on column adsorption of Cr(VI) was obtained with parameter of 6 cm of bed depth, 5 mL min^{-1} of flow rate and 50 mg L^{-1} initial Cr(VI) concentration.

Author contributions

Mochamad L. Firmansyah: conceptualization, methodology, investigation, writing – original draft, visualization, funding acquisition; Thalabul Ilmi: investigation; Rino R. Mukti: writing – review & editing, supervision, resources; Patmawati: writing – review & editing, supervision; Masahiro Goto: writing – review & editing, resources.

Conflicts of interest

The authors declare that they have no known competing financial or non-financial interests or personal relationships that could have appeared to influence the work reported in this paper.

Acknowledgements

This work was supported by Universitas Airlangga under grant Hibah Riset Mandat 2020 [395/UN3.14/PT/2020]. The author grateful towards Central Laboratory of Universitas Islam Indonesia, Yogyakarta for the assistance in the adsorbent characterization, and to CV. Chimultiguna for providing the chitosan for the present study.

References

1 A. S. Ayangbenro and O. O. Babalola, *Int. J. Environ. Res. Public Health*, 2017, 14.
2 P. K. Samantaray, S. Indrakumar, K. Chatterjee, V. Agarwal and S. Bose, *Nanoscale Adv.*, 2020, **2**, 2824–2834.
3 Ministry of Environment and Forestry of The Republic of Indonesia, *Peraturan Menteri Lingkungan Hidup RI No. 5 Tahun 2014 Tentang Baku Mutu Air Limbah*, 2014.
4 P. Sharma, S. P. Singh, S. K. Parakh and Y. W. Tong, *Bioengineered*, 2022, **13**, 4923–4938.
5 K. C. K. T. Matsuura and E. D. A. Ethylenediamine, *Appl. Water Sci.*, 2018, **8**, 1–30.
6 G. Crini, E. Lichtfouse, L. Wilson, N. Morin-crini, G. Crini, E. Lichtfouse, L. Wilson and N. M. Conventional, *Environ. Chem. Lett.*, 2019, **17**, 195–213.
7 H. El Knidri, R. Belaabed, A. Addaou, A. Laajeb and A. Lahsini, *Int. J. Biol. Macromol.*, 2018, **120**, 1181–1189.
8 M. Vakili, S. Deng, G. Cagnetta, W. Wang, P. Meng, D. Liu and G. Yu, *Sep. Purif. Technol.*, 2019, **224**, 373–387.
9 G. Ohemeng-Boahen, D. D. Sewu, H. N. Tran and S. H. Woo, *Colloids Surf., A*, 2021, **625**, 126911.
10 H. Karimi-Maleh, S. Ranjbari, B. Tanhaei, A. Ayati, Y. Orooji, M. Alizadeh, F. Karimi, S. Salmanpour, J. Rouhi, M. Sillanpää and F. Sen, *Environ. Res.*, 2021, **195**, 110809.
11 A. Santhana Krishna Kumar, T. Gupta, S. S. Kakan, S. Kalidhasan, Manasi, V. Rajesh and N. Rajesh, *J. Hazard. Mater.*, 2012, **239–240**, 213–224.
12 A. Shekhawat, S. Kahu, D. Saravanan and R. Jugade, *Int. J. Biol. Macromol.*, 2015, **80**, 615–626.
13 A. Shekhawat, S. Kahu, D. Saravanan and R. Jugade, *Int. J. Biol. Macromol.*, 2017, **104**, 1556–1568.
14 T. Monir, A. Shahr El-Din, Y. El-Nadi and A. Ali, *Radiochim. Acta*, 2020, **108**, 649–659.
15 X. Huang, S. Feng, G. Zhu, W. Zheng, C. Shao, N. Zhou and Q. Meng, *Int. J. Biol. Macromol.*, 2020, **149**, 882–892.
16 S. Ranjbari, B. Tanhaei, A. Ayati and M. Sillanpää, *Int. J. Biol. Macromol.*, 2019, **125**, 989–998.
17 X. Lin, J. Liu, S. Wan, X. He, L. Cui and G. Wu, *Int. J. Biol. Macromol.*, 2019, **136**, 35–47.
18 F. Atefi, M. T. Garcia, R. D. Singer and P. J. Scammells, *Green Chem.*, 2009, **11**, 1595.
19 M. L. Firmansyah, A. T. N. Fajar, W. Yoshida, T. Hanada and M. Goto, *J. Chem. Eng. Jpn.*, 2020, **53**, 1–8.
20 S. Kahu, D. Saravanan and R. Jugade, *Water Sci. Technol.*, 2014, **70**, 2047–2055.
21 K. K. Onchoke and S. A. Sasu, *Adv. Environ. Chem.*, 2016, **2016**, 1–10.
22 J. Song, S. A. Messele, L. Meng, Z. Huang and M. Gamal El-Din, *Water Res.*, 2021, **194**, 116930.
23 D. Wanule, J. V. Balkhande, P. U. Ratnakar, a. N. Kulkarni and C. S. Bhowate, *Int. J. Eng. Sci. Innov. Technol.*, 2014, **3**, 299–304.
24 D. Cholico-gonzalez, M. Avila-rodriguez, G. Cote and A. Chagnes, *J. Mol. Liq.*, 2013, **187**, 165–170.

© 2022 The Author(s). Published by the Royal Society of Chemistry

Open Access Article. Published on 11 April 2022. Downloaded on 9/19/2024 3:12:51 PM.
This article is licensed under a Creative Commons Attribution-NonCommercial 3.0 Unported Licence.

25 M. C. Fournier-Salaün and P. Salaün, *Cent. Eur. J. Chem.*, 2007, **5**, 1084–1093.
26 A. Sanchez-Hachair and A. Hofmann, *C. R. Chim.*, 2018, **21**, 890–896.
27 C. lu Jiang, R. Wang, X. Chen, L. gen Zheng and H. Cheng, *J. Cent. South Univ.*, 2021, **28**, 1652–1664.
28 B. S. Cunha, R. A. Bataglioli, T. B. Taketa, L. M. Lopes and M. M. Beppu, *J. Environ. Chem. Eng.*, 2019, **7**, 103181.
29 Y. Jiao, D. Han, Y. Lu, Y. Rong, L. Fang, Y. Liu and R. Han, *Desalin. Water Treat.*, 2017, **77**, 247–255.
30 S. Lagergreen, *Z. Chem. Ind. Kolloide*, 1907, **2**, 174–175.
31 Y. Ho and G. McKay, *Process Biochem.*, 1999, **34**, 451–465.
32 Y. Chen, J. Tang, S. Wang, L. Zhang and W. Sun, *Chem. Eng. J.*, 2021, **425**, 131474.
33 D. Özmen, *J. Turk. Chem. Soc., Sect. B*, 2021, **4**, 47–56.
34 H. Qiu, L. Lv, B. C. Pan, Q. J. Zhang, W. M. Zhang and Q. X. Zhang, *J. Zhejiang Univ., Sci., A*, 2009, **10**, 716–724.
35 A. Kong, Y. Ji, H. Ma, Y. Song, B. He and J. Li, *J. Cleaner Prod.*, 2018, **192**, 801–808.
36 A. Dada, A. Olalekan, A. Olatunya and O. Dada, *IOSR J. Appl. Chem.*, 2012, **3**, 38–45.
37 P. Thilagavathy and T. Santhi, *BioResources*, 2014, **9**, 3805–3824.
38 A. A. Inyinbor, F. A. Adekola and G. A. Olatunji, *Water Resour. Ind.*, 2016, **15**, 14–27.
39 M. G. El-Desouky, M. A. El-Bindary and A. A. El-Bindary, *Vietnam J. Chem.*, 2021, **59**, 341–361.
40 S. Iftekhar, D. L. Ramasamy, V. Srivastava, M. B. Asif and M. Sillanpää, *Chemosphere*, 2018, **204**, 413–430.
41 A. L. Taka, E. Fosso-Kankeu, K. Pillay and X. Y. Mbianda, *Environ. Sci. Pollut. Res.*, 2018, **25**, 21752–21767.
42 E. Fosso-Kankeu, H. Mittal, F. Waanders and S. S. Ray, *J. Ind. Eng. Chem.*, 2017, **48**, 151–161.
43 R. Niwas, U. Gupta, A. A. Khan and K. G. Varshney, *Colloids Surfaces A Physicochem. Eng. Asp.*, 2000, **164**, 115–119.
44 F. E. Soetaredjo, Y. H. Ju, S. Ismadji and A. Ayucitra, *Desalin. Water Treat.*, 2017, **82**, 188–200.
45 M. Li, S. Tang, Z. Zhao, X. Meng, F. Gao, S. Jiang, Y. Chen, J. Feng and C. Feng, *Chem. Eng. J.*, 2020, **386**, 123947.
46 H. Patel, *Appl. Water Sci.*, 2019, **9**(45), DOI: **10.1007/s13201-019-0927-7**.
47 S. Kahu, A. Shekhawat, D. Saravanan and R. Jugade, *Int. J. Environ. Sci. Technol.*, 2016, **13**, 2269–2282.
48 A. S. K. Kumar, S. Sharma, R. S. Reddy, M. Barathi and N. Rajesh, *Int. J. Biol. Macromol.*, 2015, **72**, 633–639.
49 H. Ren, B. Li, M. Neckenig, D. Wu, Y. Li, Y. Ma, X. Li and N. Zhang, *Carbohydr. Polym.*, 2019, **207**, 737–746.
50 Z. Lou, S. Xing, X. Xiao, W. Shan, Y. Xiong and Y. Fan, *Hydrometallurgy*, 2018, **179**, 141–148.

© 2022 The Author(s). Published by the Royal Society of Chemistry